npj | quantum materials

Article

Published in partnership with Nanjing University

https://doi.org/10.1038/s41535-026-00942-z

Kugel-Khomskii materials

Check for updates

Erik Koch[1] & Eva Pavarini[2] ✉

The Kugel-Khomskii super-exchange mechanism for orbital ordering is a pillar of orbital physics. Besides orbital phase transitions, it can give rise to a plethora of emergent phenomena, from exotic magnetic states, orbital-liquid phases, hidden order and much more. Yet, to identify real systems in which orbital-ordering arises purely from the Kugel-Khomskii mechanism has been a challenge. The first obstacle was that ions with orbital degrees of freedom are also of the Jahn-Teller kind. This poses a chicken-and-egg problem: electronic ordering can give rise to distortions and distortions can give rise to orbital ordering. This problem was eventually solved, showing that the two effects can be indeed disentangled. From this the next obstacle emerged: lattice distortions are very efficient in freezing orbital fluctuations, hampering the effects of orbital super-exchange. Thus, in most systems, orbital ordering occurs well above T_{KK}, the critical temperature at which super-exchange can drive it. Representative Kugel-Khomskii systems were recently identified, however. The understanding gained provides guidelines for finding Kugel-Khomskii materials. It also indicates that experimental signatures of the Kugel-Khomskii mechanism should be mostly searched via the primary effect, electronic and magnetic properties, rather than the secondary effect, lattice distortions.

About 50 years ago, Kugel and Khomskii (KK) wrote a seminal paper[1] that revolutionized our understanding of the physics of transition-metal compounds (TMCs). In that work, it was shown that in a Mott system with orbital degrees of freedom, orbitals can behave as interacting pseudospins, forming broken-symmetry ground-states—basically in the same way as local spins do. Candidate materials were $LaMnO_3$ and $KCuF_3$, two perovskites in which orbital degrees of freedom stem from the partially filled e_g shells. The idea that orbitals can order spontaneously via a purely electronic mechanism was very exciting. Accordingly, orbital-ordering (OO) became in short recognized as a universal phenomenon, and one of fundamental importance for understanding strongly-correlated transition metal-oxides. The new insight led to the postulation and identification of a plethora of additional emergent states: orbital liquid phases[2], hidden magnetic order[3], Higgs-like bosonic excitations[4], spin-orbital entanglement[5] and much more. It is now established that the interplay between orbital, spin and lattice degrees of freedom, i.e., *orbital physics*[6–12], is key to understanding the properties of many correlated TMCs, not only in the insulating but also in the metallic regime, as in the case of Hund's metals.

There is a catch, however. The fact that orbital degeneracy can lead to a global symmetry reduction was already pointed out in the early days of quantum mechanics. The microscopic mechanism identified was, however, very different: the electron-phonon interaction, via the Jahn–Teller (JT) effect[13]. Ions with partially filled d shells and orbital degrees of freedom (Fig. 1), key to KK super-exchange, are also Jahn–Teller active (Fig. 2). The two mechanisms can, and usually do, result in the same final state. To complicate the matter, a co-operative JT distortion is the expected *secondary* effect of KK orbital ordering[1]. This defines a classic chicken-and-egg problem. The latter sparked a heated debate on the origin of OO in materials, till eventually it was shown that the two mechanisms can indeed be disentangled[14]. In this paper, after a brief exposition of the original problem and its complexity, we will discuss the conclusions that can be drawn from the solution of the chicken-and-egg problem; from the understanding gained, we then provide guidelines for finding actual Kugel–Khomskii materials.

Results

Kugel–Khomskii orbital ordering

In correlated systems, magnetic ordering can arise without an actual symmetry reduction of the Hamiltonian. In the simplest form, this phenomenon is described by the single-band Hubbard model

$$H = -t \sum_{\langle ij \rangle} \sum_{\sigma} c^{\dagger}_{i\sigma} c_{j\sigma} + U \sum_{i} n_{i\uparrow} n_{i\downarrow} \qquad (1)$$

at half-filling. The double occupations of a given site cost energy U. Thus, in the atomic limit, electrons behave as local spins $\mathbf{S}_i$ (with $S_i = 1/2$), and the degeneracy of the ground manifold for N sites is 2^N. For small but finite t/U, at low energy, the local spins remain well defined, but start to interact via the emergent antiferro (AF) magnetic coupling $J = 4t^2/U$. The latter arises from virtual excitations which, due to the Pauli principle, are only possible for an alternating arrangement of neighboring spins.

[1]Jülich Supercomputing Centre, Forschungszentrum Jülich, Jülich, Germany. [2]Peter Grünberg Institut, Forschungszentrum Jülich, Jülich, Germany. ✉e-mail: e.pavarini@fz-juelich.de

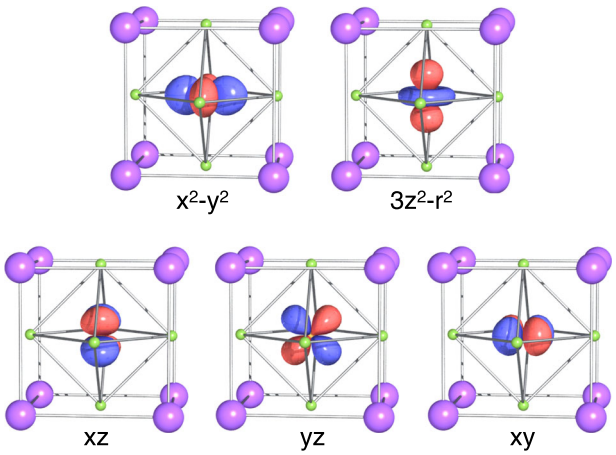


Fig. 1 | Transition-metal 3*d* orbitals in a perovskite unit cell. The figure shows an ideal perovskite ABC_3 structure. Violet spheres: cations (A=La, K,...). Green spheres: anions (C, typically O or F). The 3*d* orbitals are centered on the 3d metal site B. They are split into e_g orbitals (x^2-y^2 and $3z^2-r^2$) and t_{2g} orbitals (xy,xz,yz). Red and blue lobes indicate the positive and negative sign of the wavefunction.

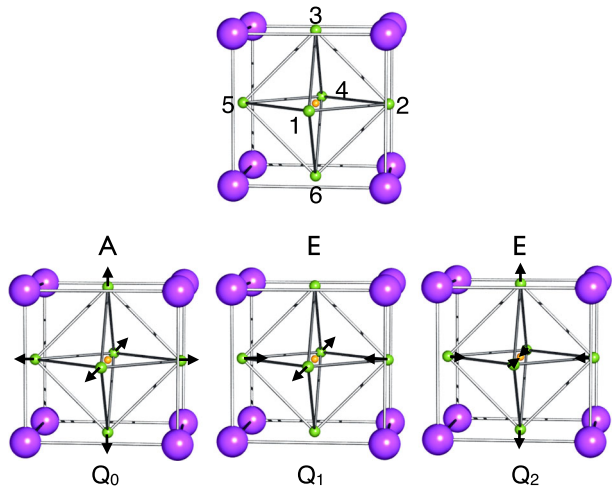


Fig. 2 | Phononic modes coupling to e_g electrons in a perovskite. Top: the unit cell of an ideal cubic perovskite with structure ABC_3. Violet spheres: cations (A=La, K,...). Green spheres: anions (C, typically O or F). Yellow spheres: 3*d* metal. Bottom: the phononic modes coupling to e_g electrons, A_g (Q_0) and E_g (Q_1, Q_2). The black arrows indicate the displacements of the C atoms characterizing the mode. The remaining modes (not shown) have symmetry T_1 and T_2, and do not couple to e_g electrons.

The half-filled Hubbard model can be then mapped onto the effective Heisenberg Hamiltonian

$$H = \Gamma \sum_{\langle ij \rangle} \left(\mathbf{S}_i \cdot \mathbf{S}_j - \tfrac{1}{4} \right), \tag{2}$$

where $\langle ij \rangle$ here identifies inequivalent pairs of neighboring transition-metal sites. In TMCs, the hopping integral t between transition-metal ions is mediated by anion p states (e.g., from the first-neighbor oxygen or fluorine atoms, see Fig. 1): the mechanism leading to AF magnetic order at a temperature $T_N \propto \Gamma$ is thus known as super-exchange (SE).

Kugel and Khomskii observed that, in a Mott insulator with orbital degrees of freedom, the same mechanism leads to the formation of interacting orbital pseudo-spins. In fact, for the case of two degenerate e_g orbitals (Fig. 1, top), with Hubbard model

$$H = -t \sum_{\langle ij \rangle} \sum_{m\sigma} c^{\dagger}_{im\sigma} c_{jm\sigma} + U \sum_{im} n_{im\uparrow} n_{im\downarrow} + \tfrac{1}{2} U \sum_{i\sigma\sigma'} \sum_{m \neq m'} n_{im\sigma} n_{im'\sigma'}, \tag{3}$$

where m is the orbital index, the SE Hamiltonian takes the form

$$H = 2\Gamma \sum_{\langle ij \rangle} \left[\left(\mathbf{S}_i \cdot \mathbf{S}_j + \tfrac{1}{4} \right) \left(\mathbf{O}_i \cdot \mathbf{O}_j + \tfrac{1}{4} \right) - \tfrac{1}{4} \right], \tag{4}$$

where the $\mathbf{O}_i$ are the spin-1/2 type operators acting in orbital space, and thus describing the orbital pseudospin. This means that pseudospins can order spontaneously at a critical temperature $T_{KK} \propto \Gamma$, the same way that spins do. The order parameter for an OO transition is p_o, the orbital polarization, i.e., the difference in occupation of the natural orbitals; this is the orbital analog of the magnetization m_z. Furthermore, the model makes explicit how OO directly affects magnetic ordering: ferro-OO favors AF-magnetic order; this is a realization of the so-called Goodenough-Kanamori rules[15–20]. In the original work of Kugel and Khomskii, candidate materials were the two perovskites $KCuF_3$ (e_g^3 configuration) and $LaMnO_3$ ($t_{2g}^3 e_g^1$ configuration), for which the orbital degrees of freedom in question stem from the e_g states of Cu or Mn. Experimentally, both systems have an orbitally-ordered ground state in line with the predictions from the Kugel–Khomskii super-exchange Hamiltonian, and their magnetic phases can be well understood starting from such orbitally-ordered states.

The conclusion that $KCuF_3$ and $LaMnO_3$ are KK materials is, however, at this point, premature. First, a direct experimental proof—as provided, e.g., from the observation of a purely electronic orbital-order transition at a critical temperature—remains elusive, differently than in the case of a purely magnetic transition. The experimental hallmark of electronic OO is typically the secondary effect of ordering, also predicted in the work of Kugel and Khomskii: the cooperative JT-like lattice distortion (see Fig. 2) associated with the broken symmetry phase[1]. Figure 3 shows such lattice distortion in the case of $KCuF_3$, with long and short CuF bonds alternating at Cu sites. In this view, the orbital-order transition temperature is identified with the structural transition temperature, $T_{OO} \sim T_s$, with the underlying implication that $T_{KK} \sim T_{OO} \sim T_s$. However, as previously mentioned, there is another path to distortions, the JT mechanism. In the conventional JT picture, for a perovksite structure with partially filled e_g shells, the relevant co-operative phononic JT modes are the E_g = (Q_1, Q_2), shown in Fig. 2. Once a JT distortion is present, the coupling to these modes results in a static crystal-field (CF) splitting ε_{CF}; electronic orbital ordering can then arise from the latter, acting as a static external field in orbital space[13,20]. The CF splitting can even be small compared to the band-width, since its effects are enhanced by Coulomb repulsion[21,22]. In the JT picture, $T_{JT} \sim T_{OO} \sim T_s$, where T_{JT} is the critical transition temperature for the JT transition from classical electron-lattice coupling. Thus, the bare onset of the cooperative distortion does not allow distinguishing between a purely electronic and lattice-mediated mechanism: the two mechanisms usually lead to a similar type of ordering, shown in Fig. 3 for $KCuF_3$. A further complication is that, in most cases, an actual transition from the highly symmetric (with orbital degeneracy) phase to a lower symmetry phase is basically never observed; more common are changes from a distorted structure to another distorted structure in rather complex phase diagrams.

Since the distortion alone (i.e., the result of both effects, the final state) is not sufficient to determine the mechanism, a number of questions need to be addressed. How do we disentangle the two mechanisms in this complex situation? How do we identify true KK materials? How strong is orbital super-exchange in orbitally degenerate strongly-correlated systems? Last but not least, what explains the fact that in most systems the ordering temperature for orbitals, $T_{OO} \sim T_s$, is much larger than the ordering temperature for spins, T_N? An extreme case in this sense is $KCuF_3$, which orders magnetically at $T_N \sim 40$ K, but exhibits a JT-like distortion till melting temperature. In $LaMnO_3$, the magnetic critical temperature leading to A-type anti-ferro magnetic order is $T_N \sim 140$ K; for what concerns T_{OO}, initial experiments pointed to distortions disappearing at $T_s^* \sim 800$ K[23,24]; later experiments have however shown that the distortions persist in nano-

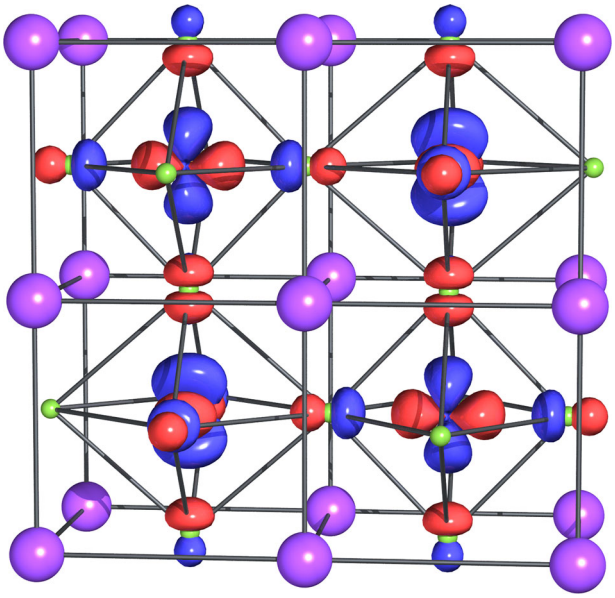


Fig. 3 | Orbital ordering (hole orbitals) in $KCuF_3$. Orbital ordering in the Jahn–Teller distorted perovskite $KCuF_3$. The electronic configuration is $t_{2g}^6 e_g^3$; the orbitals shown are the unoccupied ones (hole orbitals). Red and blue lobes indicate the positive and negative sign of the wavefunction. The structure exhibits a co-operative Jahn–Teller distortion with long and short planar CuF bonds alternating in all directions. Violet spheres: K. Green spheres: F.

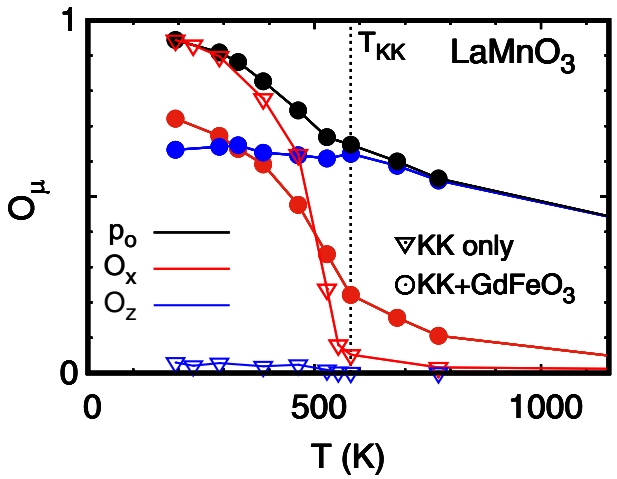


Fig. 4 | Orbital-ordering transition in $LaMnO_3$. Orbital-ordering transition in $LaMnO_3$, in the ideal case with no co-operative JT distortion, but with (circles) and without (triangles) $GdFeO_3$ distortion. The figure shows the expectation values O_μ of the pseudo-spin operators $\hat{O}_\mu$, the orbital analog of the spin operators $\hat{S}_\nu$. The label $\mu = x, z, y$ indicates the three components of the tensor; among these, $\hat{O}_y$ does not contribute since the orbitals are real and its expectation value is zero. The operators are normalized to their maximum, so that $0 < O_\mu < 1$. Red circles and red triangles: O_x. Blue circles and blue triangles: O_z. Black circles: orbital polarization, $p_o(T) = \langle \hat{O}_z \rangle + \tan(\theta/2)\langle \hat{O}_x \rangle$. The results for no $GdFeO_3$ distortion (triangles) show the ideal KK transition at temperature T_{KK} (vertical dotted line); such transition occurs in the $\hat{O}_x$ channel. In the presence of $GdFeO_3$ distortion (circles), the crystal-field splitting partially polarizes both $\hat{O}_z$ and $\hat{O}_x$ already for $T > T_{KK}$. When $T < T_{KK}$ the polarization remains constant in the $\hat{O}_z$ channel (frozen by the crystal-field splitting) but it rises rapidly in the KK channel $\hat{O}_x$.

clusters up to melting temperatures[25–27], making the 800 K transition rather a structural order-to-disorder transition, and shifting T_{OO} to above 1000 K. In the KK picture both T_{KK} and T_N are proportional to the super-exchange scale I; a systematic large difference between the two begs for an explanation.

Solving the chicken-and-egg problem

The chicken-and-egg problem was first solved in ref. 14 for $KCuF_3$. It was shown that it is possible to disentangle the two competing mechanisms by constructing a series of idealized structures with reduced JT distortions. For each of these structures, the corresponding Hubbard model was built, and the evolution of the OO order parameter with temperature was obtained; the calculations were based on a many-body approach, (cluster) dynamical mean-field theory (DMFT) with a numerically exact quantum Monte Carlo (QMC) impurity solver, a method that provides an upper limit for the transition temperature. Within this approach, if the CF splitting, ε_{CF}, is much larger than the KK energy scale $k_B T_{KK}$, the orbital polarization is close to its maximum, $p_o(T) \sim 1$, up to very high temperatures. Decreasing the distortions reduces ε_{CF}, and eventually a crossover region is found, with ε_{CF} playing the role of an external field. Finally, a pure KK transition is found in the zero-distortion limit. For $KCuF_3$, the numerical results obtained in the way described yield $T_{KK} \sim 350$ K. Experimentally, distortions in this system persist, however, till the melting temperature[28]. The unexpected conclusion is thus that, in $KCuF_3$, the KK mechanism *alone* cannot explain ordering above T_{KK}, even though the SE interaction is sizable and contributes to stabilizing orbital ordering. Hence, $KCuF_3$ is *not* a true KK system.

The case of $LaMnO_3$ is more complex. The first complication arises from the fact that the electronic configuration is $t_{2g}^3 e_g^1$; hence, the t_{2g} electrons also play a role. To a good approximation, however, due to the Hund's rule coupling, the latter act as effective spins 3/2, locally aligning the e_g electrons via the ferromagnetic Coulomb exchange[29]. The second complication is that, in the experimental structure, a $GdFeO_3$-type distortion is present. The latter is key for the electronic properties, since it sizably reduces the band-width. In $LaMnO_3$, it also induces a CF splitting; because of the latter one cannot extract T_{KK} in the same way as it was done for $KCuF_3$: the order parameter in fact always exhibits a cross-over behavior, even in the limit of zero JT-distortion. The signature of the KK transition is thus rather the rotation of the occupied orbital away from the $GdFeO_3$-type crystal-field state and toward the KK model prediction. Alternatively, one can analyze the behavior in terms of the irreducible tensorial components of the order parameter. For $LaMnO_3$, this decomposition is simply $p_o(T) = \langle O_z \rangle + \tan(\theta/2)\langle O_x \rangle$; the component $\langle O_z \rangle$ is controlled by the $GdFeO_3$-type CF splitting, and changes smoothly with temperature, while the SE transition at T_{KK} appears as a sharp increase of $\langle O_x \rangle$; because of the CF, the expectation value of $\langle O_x \rangle$ never reaches its maximum, however (frustration). This is shown in Fig. 4. The procedure described yields $T_{KK} \sim 600$ K, much larger than for $KCuF_3$; this is very close to $T_s^* \sim 800$ K, the temperature at which a disordered phase with nanocluster forms[25–27] (orbital order melting); the JT distortion itself, however, persists in the nanoclusters till melting temperatures, i.e., T_s is larger than 1000 K. The overall conclusion, therefore, is the same as for $KCuF_3$[30–32]: SE alone is *not* sufficient to explain the distortions in the whole temperature range in which they are observed. Nonetheless, since $T_{KK} \sim T_s^*$, one might wonder if the onset of the orbital melting transition at T_s^* is indeed controlled by orbital SE, since the latter contributes to the energy gain stabilizing orbital ordering. The answer to this question comes from experimental trends. Orbital melting is observed in other systems of the $ReMnO_3$ family[33–36], with T_s^* sharply increasing with decreasing rare-earth ionic radius. Theoretical calculations show that T_{KK} itself is weakly dependent on the rare-earth ionic radius[31], however. These results mean that the KK mechanism is also not the critical interaction controlling the onset of the order-to-disorder transition.

Summarizing, after a solution to the chicken-and-egg problem was found, it became clear that the two systems originally proposed, and sometimes still quoted, as paradigmatic examples for spontaneous electronic orbital ordering, in reality, cannot be considered true KK materials, even if the orbital SE interaction is indeed very strong in these compounds, in particular in the case of $LaMnO_3$. In fact, experimentally, the JT-type distortion, and with it orbital ordering, stabilizes at a temperature $T_s \gg T_{KK}$;

hence, electron-phonon coupling effects dominate. A similar conclusion was obtained for other classes of e_g systems, such as layered perovskites[37].

Thermally-assisted ordering

Taking the opposite viewpoint, can one explain the experimental structure of orbitally ordered systems with the JT mechanism alone? To address this question, it is useful to consider the case of $KCuF_3$, which only shows JT-type distortions and maintains its crystalline form till extreme temperatures. Is $KCuF_3$ a true JT system?

Let us first recall what is expected in this case. In the Landau picture, phase transitions are the result of the competition between energy and entropy. The ordered phase has lower energy, and the disordered larger entropy; order thus vanishes at a critical temperature, here $T_{\rm JT}$. Furthermore, the order parameter showing the transition is the JT distortion, $\delta_{\rm JT}$. In the case of an e_g cubic perovskite, $\delta_{\rm JT}$ can be identified with the deformation from the JT phononic mode Q_1, shown in Fig. 2; hence $\delta_{\rm JT} = (l - s)/2(l + s)$, where l and s are the long and short bonds between the transition metal and the anion. It was thus very surprising when it was found experimentally that in $KCuF_3$, $\delta_{\rm JT}$ *increases*, instead of decreasing, with temperature[28], so that in practice no finite value can be assigned to $T_{\rm JT}$. From the theory side, equally surprising was the fact that such behavior is perfectly reproduced by total-energy density-functional-type calculations, both within the GGA and GGA $+U$ functionals[38], and that the latter are furthermore in excellent agreement with many-body DMFT results[39].

The reason is a new mechanism leading to distortions and thus to orbital ordering, identified in ref.[38]. In fact, the Landau picture of phase transitions assumes that the energy difference between the ordered and disordered phases does not change with temperature. However, in the case of $KCuF_3$, the latter sizably increases with temperature. The behavior of the systems remains thus dominated by energy, rather than entropy, and this remains true up to melting temperatures. This is because the magnitude of the distortion is not determined by the JT interaction but rather by the Born–Mayer repulsion: the short CuF distance remains unchanged increasing the temperature, and in first approximation corresponds to a picture of touching ions. At the same time, the long CuF distance progressively increases due to lattice expansion. Thus, it is the symmetric A mode controlling the lattice constant that matters (Fig. 2) rather than the two JT modes of symmetry E_g. Remarkably, the length of the short CuF bond turns out to be about the same in most known CuF systems, indicating that the mechanism just described is very general in strongly ionic materials. Furthermore, this mechanism not only explains the absence of a true JT transition in $KCuF_3$, but also opens up the possibility of an inverted transition in closed shell systems, where the ordered phase only appears *above* a critical temperature.

Finding true Kugel–Khomskii systems

The understanding of the mechanisms of orbital ordering allows us to formulate materials-design guidelines for the search of KK systems, i.e., materials whose properties are dominated by superexchange. As we have seen, e_g systems are prone to sizable static distortions, via a combination of JT and Born–Mayer effects, leading to large CF splittings. This is partially due to the fact that e_g electrons form σ bonds with anionic p states; hence, they strongly interact with the heavy lattice. Furthermore, for e_g systems, the type of instabilities that can arise from KK super-exchange and JT effect are essentially the same, since there are only two pseudospin operators that contribute. This suggests a few criteria that can serve as guidelines for finding true KK materials:

- Focus on the primary effect, electronic properties, rather than on the secondary effect, the onset of distortions. Most systems with orbital degrees of freedom exhibit some form of distortion. Accordingly, the orbital ordering temperature $T_{\rm OO}$ should be defined as the temperature at which orbital fluctuations are suppressed; operatively, one can use the criterion $p_o(T_{\rm OO}) = 0.5$; this choice stems from the fact that the orbital polarization is normalized to its maximum value so that $0 < p_o < 1$.
- On the other hand, *changes* in distortions concomitant with the formation of new orbital phases can be significant.
- Complex ordering in the absence of distortions provides an alternative path.
- Systems with more than two orbital degrees of freedom are more likely to exhibit KK super-exchange effects even in the presence of distortions. This is because some super-exchange channels might still be free, allowing for an orbital ordering transition, even if others are frozen by the CF splitting.
- Systems with weaker electron-phonon coupling (weak JT-active ions) are better candidates.
- Stronger is not necessarily better. A very large SE interaction is not a guarantee for KK orbital ordering, since in most cases, when SE is very large, CF effects are even larger.

These criteria suggest systems with partially filled t_{2g} shells as better candidates, e.g., t_{2g}^n perovskites. The latter form π bonds and are thus typically more weakly coupled to the lattice than e_g electrons. With three orbital degrees of freedom (pseudospin $S = 1$), the KK Hamiltonian offers a larger number of options for breaking orbital degeneracy via orbital ordering. These materials are also more prone to electronic phase transitions at low temperatures.

General super-exchange models for materials

From the theory side, to go beyond the case of e_g orbitals requires generalizing the approach. The first step consists in expanding the super-exchange Hamiltonian into irreducible tensor components[40–43]. The general form of the interaction is

$$\hat{H}_{\rm SE} = \frac{1}{2}\sum_{i,j}\hat{H}^{\rm SE}_{i,j} \tag{5}$$

$$= \frac{1}{2}\sum_{ij}\sum_{rr'\mu\mu'}\sum_{qq'\nu\nu'}\hat{\tau}_i^{r\mu;q\nu}\tilde{D}^{ij;q\nu q'\nu'}_{r\mu,r'\mu'}\hat{\tau}_j^{r'\mu';q'\nu'}, \tag{6}$$

where $\hat{\tau}_i^{r\mu;q\nu}$ are irreducible pseudo-spin tensors acting on the pseudospins; q is the spin rank and r the orbital rank; the corresponding components are ν (for the spin rank q) and μ (for the orbital rank r). In this expansion, the range of possible q and r values is determined by the form of the tensor operators

$$\hat{\tau}_i^{r\mu;q\nu} = \sum_{mm'}\sum_{\sigma\sigma'}\alpha^{r\mu}_{m,m'}\gamma^{q\nu}_{\sigma,\sigma'}c^{\dagger}_{im\sigma}c_{im'\sigma'}, \tag{7}$$

where $\alpha^{r\mu}_{m,m'}$ and $\gamma^{q\nu}_{\sigma,\sigma'}$ are numerical coefficients. For the spin indices, the only possible linearly independent combinations are given by $\gamma^{q\nu}_{\sigma,\sigma'} = \delta_{q,0}\langle\sigma|\hat{1}|\sigma'\rangle + \delta_{q,1}\langle\sigma|\hat{\sigma}_\nu|\sigma'\rangle$, where $\hat{1}$ is the identity matrix and $\hat{\sigma}_\nu$ are Pauli matrices; hence the spin rank is either $q = 0$ or $q = 1$; the associated components are $\nu = 0$ ($q = 0$), $\nu = -1, 0, 1$ ($q = 1$). This is independent of the effective magnetic moment $S_{\rm eff}$ of the ground multiplet; the latter (normalization aside) determines, however, the *expectation value* of the operator $\mathbf{S}_i \cdot \mathbf{S}_i \propto \sum_\nu (\tau_i^{00;1\nu})^2$. In a similar way, for the orbital components, the maximum rank depends on the number of orbital degrees of freedom included explicitly in the model. For e_g electrons (a doublet), the maximum orbital rank is $r = 1$, as for spins. For t_{2g} electrons (a triplet), it goes up to $r = 2$. Correspondingly, the components are $\mu = s$ ($r = 0$), $\mu = x, y, z$ ($r = 1$) and $\mu = xz, yz, xy, 3z^2 - r^2, x^2 - y^2$ ($r = 2$) respectively. In order to make their role clearer, it is convenient to regroup all these terms as

$$\hat{H}_{\rm SE} = \tfrac{1}{2}\sum_{i,j}\left(\hat{H}^{\rm SE}_{C_iC_j} + \hat{H}^{\rm SE}_{O_iO_j} + \hat{H}^{\rm SE}_{S_iS_j} + \hat{H}^{\rm SE}_{O_iS_iO_jS_j}\right). \tag{8}$$

and $R = r + r' = 0$; it does not contribute in the absence of charge ordering, and we will thus use it as the energy zero. $\hat{H}^{\rm SE}_{O_iO_j}$ collects all terms

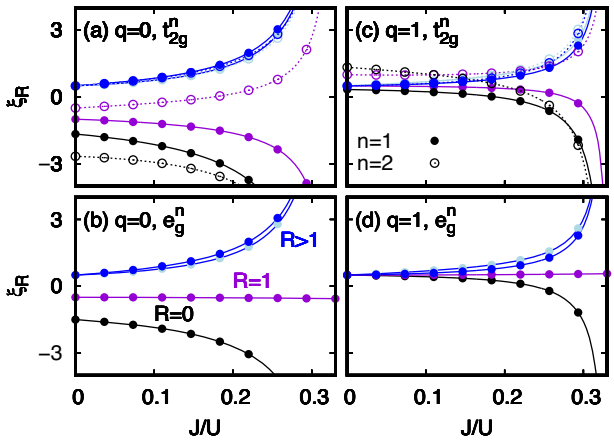


Fig. 5 | Hund's rule coupling dependence of the super-exchange expansion prefactors. The super-exchange expansion coefficients ξ_R^q (with $R = r + r'$)) as a function of J/U for the Kanamori form of the Coulomb interaction. **a**: $q = 0$, t_{2g}^n; **b** $q = 0$, e_g^n; **c** $q = 1$, t_{2g}^n; **d** $q = 1$, e_g^n. Line colors indicate the value of R (black: 0; violet: 1, blue: > 1). The functions are shown for $n = 1$ (filled circles) and $n = 2$ (open circles). The corresponding particle-hole symmetric functions ($n = 1 \rightarrow 3$ and $n = 2 \rightarrow 4$) are identical, except that they change sign for $R = 1$. Light-blue circles: complex operators with $R > 1$ that do not contribute for real wavefunctions.

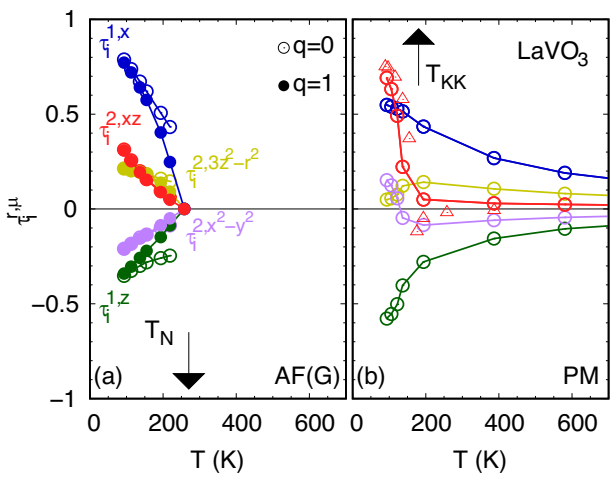


Fig. 6 | Orbital- and magnetic-ordering transitions in $LaVO_3$. Expectation value of the relevant irreducible pseudospin tensors $\hat{\tau}_i^{r\mu;qv}$ for t_{2g} electrons, calculated via dynamical mean-field theory[43]. **a** Anti-ferro (AF) magnetic transition for G-type magnetic ordering; in this structure, the local spins alternate in all directions. The black arrow indicates the transition temperature T_N. **b** Orbital-ordering transition in the paramagnetic (PM) phase. The black arrow indicates the transition temperature T_{KK}. Empty circles: $q = 0$. Filled circles: $q = 1$. Blue symbols: $\langle\tau_i^{1,x}\rangle$; green symbols: $\langle\tau_i^{1,z}\rangle$; red symbols: $\langle\tau_i^{2,xz}\rangle$; violet symbols: $\langle\tau_i^{2,x^2-y^2}\rangle$; dark yellow symbols: $\langle\tau_i^{2,3z^2-r^2}\rangle$. Empty triangles: Kugel–Khomskii transition in the ideal case (no crystal-field splitting), in the $\langle\tau_i^{2,xz}\rangle$, $q = 0$ channel. The same transition is found in the fully distorted case (red empty circles).

that determine a pure orbital transition, i.e., those for which $Q = 0$ and $R > 0$; within this group, $R = 1$ terms have the form of an orbital Zeeman interaction and are active only in distorted or layered structures. $\hat{H}^{\rm SE}_{S_iS_j}$ collects the terms with $Q > 0$ and $R = 0$; these determine a pure spin transition in the absence of orbital ordering (para-orbital phase). The rest, $\hat{H}^{\rm SE}_{O_iS_iO_jS_j}$, is from operators with both $Q > 0$ and $R > 0$; it determines spin-orbital entanglement. If the magnetic transition occurs in the presence of orbital ordering, $\hat{H}^{\rm SE}_{O_iS_iO_jS_j}$ contributes sizably to the magnetic structure as well.

The specific form of the (exact) general super-exchange model for a given system—i.e., the $\tilde{D}^{ij;qvq'v'}_{r\mu,r'\mu'}$ coefficients—can be obtained from the original multi-band Hubbard model using second-order perturbation theory and the orthogonality properties of irreducible tensors[40,41]. This approach provides both the analytic and the numerical values of the SE tensors $\tilde{D}^{ij;qvv'}_{r\mu,q'\mu'}$ in real materials at minimal computational cost. The values of the $\tilde{D}^{ij;qvq'v'}_{r\mu,r'\mu'}$ coefficients depend on various factors: *(i)* the ground multiplet, *(ii)* the hopping integrals, and *(iii)* the Coulomb tensor. For e_g and t_{2g} electrons, in the atomic limit, the latter has the Kanamori form. In the absence of spin-orbit (SO) interaction, the corresponding super-exchange tensor has been derived in refs. 40 41; in this case, one can rewrite its elements as

$$\tilde{D}^{ij;qvq'v'}_{r\mu,r'\mu'} = \frac{2\xi_R^q}{U}\,\tilde{T}^{ij}_{r\mu,r'\mu'}\delta_{q,q'}\delta_{vv'}. \tag{9}$$

Here $\tilde{T}^{ij}_{r\mu,r'\mu'}$ depends only on the hopping integrals. In a compact form,

$$\begin{aligned}\tilde{T}^{ij}_{r\mu,r'\mu'} &= \sum_{m_1,m_1'}\sum_{m_2,m_2'} t^{ij}_{m_1m_2}\,t^{ij}_{m_1'm_2'}\,C^{i;r\mu}_{m_1m_1'}\,C^{j;r'\mu'}_{m_2m_2'}\\ C^{i;r\mu}_{m_1m_1'} &= \sum_{\sigma}\left\langle 0|c_{im_1\sigma}|\hat{\tau}_i^{r\mu;00}|c^{\dagger}_{im_1'\sigma}|0\right\rangle.\end{aligned} \tag{10}$$

Instead, the ξ_R^q prefactors are functions of J/U, whose form depends on the electronic configuration and the spin rank q. They are shown in Fig. 5; for the t_{2g}^2 and t_{2g}^4 configurations we assume that the ground multiplet is a high-spin state ($S_{\rm eff} = 1$), as in the typical experimental case for the materials considered here. The left panels of Fig. 5 show that increasing J/U enhances the $\hat{H}_{O_iO_j}$ terms with $R > 1$ (blue circles, $q = 0$), driving pure KK orbital ordering and determining $T_{\rm KK}$. For spin rank $q = 1$ (right panels), Fig. 5 shows that for $J = 0$ all coefficients are positive and comparable in size. In addition, $\tilde{T}^{ij}_{00,00} > 0$; thus, the $\hat{H}_{S_iS_j}$ terms (black circles, $R = 0$) yield in this case an AF-magnetic coupling between local effective spins.

In the presence of the spin-orbit interaction, the general form of SE Hamiltonian (5) remains the same, but the $\tilde{D}^{ij;qvq'v'}_{r\mu,r'\mu'}$ tensor elements mix the spin rank components. For $3d$ systems –the classic orbital-ordering case discussed here– the SO coupling λ is typically weak in comparison to U, J and the CF splitting, and can thus be neglected in discussing the origin of orbital ordering.

Finally, the order parameter, the orbital polarization, is split into its irreducible components as $p_o(T) = \sum_{r\mu} a_{r\mu}\langle\hat{\tau}_{r\mu}\rangle$. An example of this splitting in many-body calculations is shown in Fig. 6.

The case of t_{2g}^n perovskites

Classic families of t_{2g} systems exhibiting orbital-order phenomena are cubic perovskites with the same crystal structure as $LaMnO_3$. Here, we analyze representative groups of systems in this set.

The first group is made of the t_{2g}^1 titanates, among which $LaTiO_3$ and $YTiO_3$. Theoretical calculations yield $T_{\rm KK} \sim 350$ K in both systems[40], a value similar to the one of $KCuF_3$. These systems are strongly orbitally polarized already at $T \gg T_{\rm KK}$, with $p \sim 0.7$ at 1000 K[40]. The value of $T_{\rm OO}$ is thus large, but much smaller than for $KCuF_3$, for which at the same temperature $p(T) \sim 1$ was obtained[14]. In conclusion, titanates are closer to the KK picture than $KCuF_3$, but yet the occupied orbital is determined essentially by the CF splitting, and all orbital channels are frozen.

One can use the magnetic structure of these systems to put these conclusions to the test. A peculiarity of the titanates is that their magnetic structure is very sensitive to details; for the two systems in question, while $LaTiO_3$ is a G-type antiferromagnet[44], $YTiO_3$ orders ferromagnetically (FM) with a low critical temperature[45]. FM phases are rare among Mott insulators, since they require the combined action of the Hund's rule coupling and hopping integrals to empty states. The orbital ordering obtained in DMFT calculations—with the occupied orbital essentially determined by the CF splitting—yields a magnetic structure in line with experiments (antiferromagnetic in $LaTiO_3$ and ferromagnetic in $YTiO_3$)[22,32], confirming the conclusion.

The second group of t_{2g} candidates is the $ReVO_3$ series, t_{2g}^2 perovskites. These vanadates have a rich phase diagram[46–54], with a structural phase transition (orthorhombic to monoclinic) at a relatively low temperature,

$T_s \sim 200$ K. The latter has been associated with the onset of orbital ordering ($T_s \sim T_{OO}$); orbital fluctuations, however, appear already suppressed at higher temperature, in particular for small ionic radius[54,55]. Most importantly, the vanadates exhibit a unique and remarkable phenomenon: the inversion of T_N and T_{OO} with increasing rare-earth radius up to La/Ce[51–53].

Theoretical calculations show that the relative weight of the JT and SE mechanisms in determining orbital ordering changes across the series[42,43]. In vanadates with small Re radius, orbital ordering sets in at a temperature T_{OO} which is well above $T_s > T_{KK}$; this is not the case for large Re radius, however, where $T_{KK} \sim T_{OO} \sim T_s$. The irreducible tensor decomposition shows in this situation an SE orbital transition in the *xz* channel, Fig. 6, red circles; this is similar to the transition found in the corresponding ideal undistorted material, red triangles. It is important to underline that the transition appears *in the presence* of CF splitting, which freezes certain channels, leaving, however, the key one free: $\langle \tau^{2xz} \rangle = 0$ for $T > T_{KK}$. Another way of visualizing the transition is following the evolution with temperature of the occupied orbital on the Bloch sphere: Fig. 7 shows how, lowering the temperature, the orbital moves away from the CF state, towards the KK state.

Remarkably, the experimental inversion of magnetic and orbital ordering for large Re radius (La) emerges naturally from the calculations: $T_N > T_{KK} \sim T_{OO} \sim T_s$. The reason behind such a $T_N \leftrightarrow T_{OO}$ inversion has far-reaching implications. In fact, an inversion can only occur if two conditions are satisfied. The first is $T_{OO} \sim T_{KK}$: if this does not happen, orbital ordering is determined by the high-energy scale of lattice distortions, and $T_N < T_{OO}$. This, however, is not sufficient. The second condition is that the SE term leading to a purely magnetic transition ($q = 1, r + r' = 0$) in the absence of orbital ordering must be larger than pure orbital terms. The analysis of the channel-resolved couplings (see Fig. 5, Eq. (9), Eq. (10)) shows that the t_{2g}^2 configuration helps in satisfying this condition. In vanadates, in fact, if T_{OO} was close to T_{KK} in all cases, one could find the inversion in the entire series. It is the first criterion that is not satisfied for small ionic radius (e.g., Y), i.e., the key condition defining a KK material. More in general, we can conclude from this that the very fact that in most systems $T_N \ll T_{OO}$ is evidence that pure KK materials are rare.

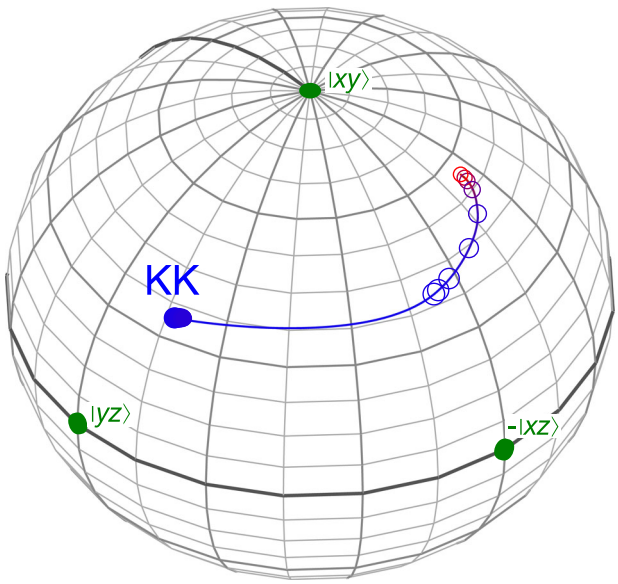


Fig. 7 | Evolution of the t_{2g} hole orbital of $LaVO_3$ as a function of temperature. The figure shows the rotation of the hole orbital from the crystal-field state at high temperature (red empty circle) towards the Kugel–Khomskii (KK) state at low temperature (filled blue circle). A t_{2g} orbital is represented as $\sin\theta\cos\phi|xz\rangle + \cos\theta|xy\rangle + \sin\theta\sin\phi|yz\rangle$, hence identified by the two angles ϕ and θ as a point on the Bloch sphere. In green we show the position on the sphere of the three t_{2g} orbitals $|xz\rangle$, $|xy\rangle$, and $|yz\rangle$.

Discussion

We started from fundamental questions: which materials can be considered of Kugel–Khomskii rather than Jahn–Teller type, and how do we identify them? The solution of the chicken-and-egg problem has provided a systematic approach to address these questions. Thanks to the combination of DMFT calculations and general irreducible tensor decompositions of super-exchange models, we can now identify which super-exchange channels are active even in the presence of static lattice distortions, and we can at the same time extract T_{KK}. The results obtained for representative families of e_g and t_{2g} materials[14,30–32,37,40–43,56] are collected in Fig. 8. The general conclusions drawn are discussed below.

First, in most TMCs with orbital degrees of freedom, KK orbital super-exchange turns out to be large. In cubic perovskites, the KK orbital order transition temperature T_{KK} ranges from about 200–300 K in t_{2g} systems up to 600–800 K in e_g manganites.

Yet, lattice distortions typically persist well above T_{KK}. In such a situation, the actual temperature T_{OO} at which orbital order forms is then larger or much larger than T_{KK}. In Fig. 8, this can be seen from the fact that most points are below the diagonal in the phase diagram, and $T_{OO} \sim T_{CF}$, the CF temperature scale $T_{CF} \sim \varepsilon_{CF}/k_B$. In these cases, even if not the driving mechanism, a large SE enhances the effects of distortions, helping to suppress orbital fluctuations. Furthermore, SE plays, of course, a key role in controlling magnetism, via the irreducible tensor terms entangling spin and orbital degrees of freedom, yielding, e.g., the Goodenough-Kanamori rules. In this respect, the effects of orbital order are most important in A-type AF magnetic structures or in FM phases, for which the pure spin-spin SE interaction term ($q = 1, r + r' = 0$), typically AF, is frustrated.

Next, the inversion of T_N and T_{OO} is rare because the standard case is $T_{KK} \ll T_{OO} \sim T_{CF}$, hence $T_N < T_{OO}$. This can be seen in Fig. 8, where the empty symbols (T_N) are almost always below the full symbols (T_{KK}). There are exceptions, however. One is the family of rare-earth vanadates; here, for large ionic radius, T_{OO} and T_{KK} come to be close to each other, so that the systems can be considered of Kugel–Khomskii kind. In this situation an inversion of magnetic and orbital ordering ($T_N > T_{OO} \sim T_{KK}$) is possible –in particular in G-type magnetic structure and the t_{2g}^2 or t_{2g}^4 configuration, which yield a larger SE spin-spin ($q = 1, r = 0$) term – and has indeed been reported experimentally[51–53].

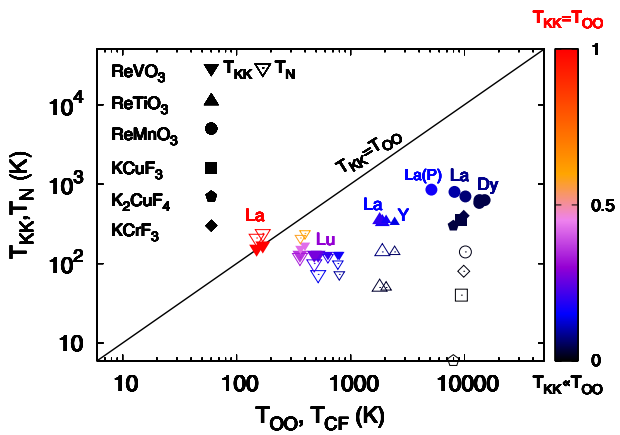


Fig. 8 | Kugel–Khomskii materials roadmap. T_{KK}, the Kugel–Khomskii temperature (filled symbols) and T_N, the magnetic transition temperature (empty symbols), in various families of orbitally ordered systems. Inverted triangles: $ReVO_3$. Triangles: $ReTiO_3$. Circles: $ReMnO_3$. Squares: $KCuF_3$. Pentagons: K_2CuF_4. Rhombus: $KCrF_3$. The critical temperatures are shown as a function of $T_{CF} \sim \varepsilon_{CF}/k_B$ and T_{OO}; the latter (represented via larger symbols) is only shown when below melting temperature. The color scale shows the T_{KK}/T_{OO} ratio. It ranges from red to black. Red: Kugel–Khomskii limit ($T_{OO} = T_{KK}$). Black: static distortion limit ($T_{OO} \gg T_{KK}$). The results shown are for a number of representative families of orbitally-ordered systems. Calculations are based on DMFT and super-exchange theory. The label La (P) indicates results under pressure (P=9 GPa).

There are a number of unexpected lessons. The first is that Kugel–Khomskii materials are not the ones proposed in the original work of Kugel and Khomskii. The second is that to identify Kugel–Khomskii systems, one has to shift the attention back to the primary effect, the electronic properties, instead of focusing on the onset of lattice distortions. This is because in most systems with orbital degrees of freedom, some distortions exist due to a combination of Jahn–Teller interaction and Born-Mayer repulsion. This also has the advantage that the same criteria apply in the presence of static or dynamical JT distortions. Experimental tools providing information on orbital occupations and their changes with decreasing temperature are key. A promising novel approach is the direct imaging of orbitals with X-rays[57,58]. Systems with a larger number of degrees of freedom are better candidates, since the distortions can freeze certain channels but leave others free. Materials with t_{2g} orbital degrees of freedom are more promising than e_g systems, and the t_{2g}^2 or t_{2g}^4 configurations are more prone than t_{2g}^1 or t_{2g}^3 to favor an inversion of T_N and T_{OO}. Complex ordering is another possible path, provided, however, that the SO interaction does not totally suppress orbital degrees of freedom. Finally, a last surprise is that a large T_{KK} alone is not sufficient to guarantee that a system is of KK type, since it is the presence of free channels, not frozen by the CF splitting, that is more important; it is indeed remarkable that Kugel–Khomskii vanadates are in fact the materials in Fig. 8 with the smallest absolute value of T_{KK}.

This article is dedicated to the memory of Daniel Khomskii, who inspired the entire work. We discussed with Daniel many of the early results on $KCuF_3$ and $LaMnO_3$; he was very interested in the outcome, even if the results were going against his original predictions. We regret that it was no longer possible to show him the more recent findings; we are sure that he would have enjoyed seeing that the mechanism he proposed more than 50 years ago has finally been proven in real systems.

Methods

Numerical techniques

The results shown are based on the DFT+DMFT method and its cluster extension. This technique combines density-functional-theory (DFT) based band-structure calculations with DMFT. DFT band-structure calculations were used in the construction of the model. The approaches employed are the NMTO method as implemented in the Stuttgart NMTO47 code[22] and the LAPW method as implemented in Wien2k[59]. The DMFT quantum-impurity solvers adopted are based on the QMC approach, Hirsch-Fye and continuous-time hybridization-expansion flavors; these codes have been developed by us[32,37,60]. For each family of materials, simulations have been performed for well-established U, J values, yielding the correct gap size and multiplet sequence, $U \sim 5$ eV and $J \sim 0.7$ eV for titanates, vanadates, and manganites, $U \sim 7$ eV for cuprates. For calculating T_{KK} we combined DMFT with the tensorial decomposition of the super-exchange interactions[40,41] and we calculated the expectation values of the key pseudospin operators.

Data availability

The data that support the findings of this study are not publicly available due to the extensive time needed to reformat them in a standard open-source format, but they are available from the corresponding author upon reasonable request.

Received: 25 April 2026; Accepted: 31 August 2026;
Published online: 16 September 2026

References

1. Kugel, K. I. & Khomskii, D. I. Crystal structure and magnetic properties of substances with orbital degeneracy. *Zh. Eksp. Teor. Fiz.* **64**, 1429 (1973).
2. Khalliullin, G. & Maekawa, S. Orbital liquid in ferromagnetic layered manganites. *Phys. Rev. Lett.* **85**, 3950 (2000).
3. Jakeli, G. & Khalliullin, G. Magnetically hidden order of Kramers doublets in d^1 Systems: Sr_2VO_4. *Phys. Rev. Lett.* **103**, 067205 (2009).
4. Jain, A. et al. Higgs mode and its decay in a two-dimensional antiferromagnet. *Nat. Phys.* **13**, 633 (2017).
5. Oleś, A. M., Khaliullin, G., Horsch, P. & Feiner, L. F. Fingerprints of orbital physics in magnetic fluctuations in manganites. *Phys. Rev. B.* **72**, 214431 (2005).
6. Tokura, Y. & Nagaosa, N. Orbital physics in transition-metal oxides. *Science* **288**, 462 (2000).
7. Khomskii, D. I. Orbital physics: glorious past, bright future. *J. Sol. Stat. Sci. Tech.* **11**, 054004 (2022).
8. Khomskii, D. I. Role of orbitals in the physics of correlated electron systems. *Phys. Scr.* **72**, CC8 (2005).
9. Khalliullin, G. Orbital order and fluctuations in Mott insulators. *Prog. Theor. Phys. Suppl.* **160**, 155 (2005).
10. Nussinov, Z. & van den Brink, J. Compass models: theory and physical motivations. *Rev. Mod. Phys.* **87**, 1 (2015).
11. Khomskii, D. I. *Transition Metal Compounds* (Cambridge University Press, 2014).
12. Chen, G. V. & Wu, C. Multi flavor Mott insulators in quantum materials and ultracold atoms. *npj Quantum Mater.* **9**, 1 (2024).
13. Jahn, H. A. & Teller, E. Stability of polyatomic molecules in degenerate electronic states - I. Orbital degeneracy. *Proc. R. Soc. A.* **161**, 220 (1937).
14. Pavarini, E., Koch, E. & Lichtenstein, A. I. Mechanism for orbital ordering in $KCuF_3$. *Phys. Rev. Lett.* **101**, 266405 (2008).
15. Goodenough, J. B. Theory of the role of covalence in the perovskite-type manganites [La,M(II)]MnO_3. *Phys. Rev.* **100**, 564 (1955).
16. Goodenough, J. B. An interpretation of the magnetic properties of the perovskite-type mixed crystals $La_{1-x}Sr_xCoO_{3-\lambda}$. *J. Phys. Chem. Solids* **6**, 287 (1958).
17. Goodenough, J. B. *Magnetism and the Chemical Bond* (Interscience, 1963).
18. Kanamori, J. Theory of the magnetic properties of ferrous and cobaltous oxides, I. *Prog. Theor. Phys.* **17**, 177 (1957).
19. Kanamori, J. Superexchange interaction and symmetry of electron orbitals. *J. Phys. Chem. Solids* **10**, 87 (1959).
20. Kanamori, J. Crystal distortion in magnetic compounds. *J. Appl Phys.* **31**, S14 (1960).
21. Pavarini, E. et al. Mott transition and suppression of orbital fluctuations in orthorhombic $3d^1$ perovskites. *Phys. Rev. Lett.* **92**, 176403 (2004).
22. Pavarini, E., Yamasaki, A., Nuss, J. & Andersen, O. K. How chemistry controls electron localization in $3d^1$ perovskites: a Wannier-function study. *New J. Phys.* **7**, 188 (2005).
23. Rodríguez-Carvajal, J. et al. Neutron-diffraction study of the Jahn-Teller transition in stoichiometric $LaMnO_3$. *Phys. Rev. B* **57**, R3189 (1998).
24. Murakami, Y. et al. Resonant X-ray scattering from orbital ordering in $LaMnO_3$. *Phys. Rev. Lett.* **81**, 582 (1998).
25. Sánchez, M. C., Subías, G., García, J. & Blasco, J. Cooperative Jahn-Teller phase transition in $LaMnO_3$ studied by X-ray absorption spectroscopy. *Phys. Rev. Lett.* **90**, 045503 (2003).
26. Qiu, X., Proffen, T., Mitchell, J. F. & Billinge, S. J. L. Orbital correlations in the pseudocubic *O* and rhombohedral *R* phases of $LaMnO_3$. *Phys. Rev. Lett.* **94**, 177203 (2005).
27. Sartbaeva, A., Wells, S. A., Thorpe, M. F., Bozin, E. S. & Billinge, S. J. L. Quadrupolar ordering in $LaMnO_3$ revealed from scattering data and geometric modeling. *Phys. Rev. Lett.* **99**, 155503 (2007).
28. Marshall, L. G. et al. Unusual structural evolution in $KCuF_3$ at high temperatures by neutron powder diffraction. *Phys. Rev. B* **87**, 014109 (2013).
29. Ahn, K. H. & Millis, A. J. Effects of magnetic ordering on the anisotropy and temperature dependence of the optical conductivity in $LaMnO_3$: a tight-binding approach. *Phys. Rev. B* **61**, 13545 (2000).
30. Pavarini, E. & Koch, E. Origin of Jahn-Teller distortion and orbital order in $LaMnO_3$. *Phys. Rev. Lett.* **104**, 086402 (2010).

31. Flesch, A., Zhang, G., Koch, E. & Pavarini, E. Orbital-order melting in rare-earth manganites: Role of superexchange. *Phys. Rev. B* **85**, 035124 (2012).
32. Flesch, A., Gorelov, E., Koch, E. & Pavarini, E. Multiplet effects in orbital and spin ordering phenomena: a hybridization-expansion quantum impurity solver study. *Phys. Rev. B* **87**, 195141 (2013).
33. Zhou, J.-S. & Goodenough, J. B. Orbital order-disorder transition in single-valent manganites. *Phys. Rev. B* **68**, 144406 (2003).
34. Zhou, J.-S. & Goodenough, J. B. Unusual evolution of the magnetic interactions versus structural distortions in RMnO$_3$ perovskites. *Phys. Rev. Lett.* **96**, 247202 (2006).
35. Dabrowski, B. et al. Structural, transport, and magnetic properties of RMnO$_3$ perovskites (R=La, Pr, Nd, Sm, ^{1}53Eu, Dy). *J. Solid State Chem.* **178**, 629 (2005).
36. Maris, G., Volotchaev, V. & Palstra, T. T. M. Effect of ionic size on the orbital ordering transition in RMnO$_{3+\delta}$. *N. J. Phys.* **6**, 153 (2004).
37. Musshoff, J., Zhang, G., Koch, E. & Pavarini, E. Linear-response description of superexchange-driven orbital ordering in K_2CuF_4. *Phys. Rev. B* **100**, 045116 (2019).
38. Sims, H., Pavarini, E. & Koch, E. Thermally assisted ordering in Mott insulators. *Phys. Rev. B* **96**, 054107 (2017).
39. Leonov, I. et al. Structural relaxation due to electronic correlations in the paramagnetic insulator $KCuF_3$. *Phys. Rev. Lett.* **101**, 096405 (2008).
40. Zhang, X.-J., Koch, E. & Pavarini, E. Origin of orbital ordering in $YTiO_3$ and $LaTiO_3$. *Phys. Rev. B* **102**, 035113 (2020).
41. Zhang, X.-J., Koch, E. & Pavarini, E. General superexchange Hamiltonians for magnetic and orbital physics in e_g and t_{2g} systems. *Phys. Rev. B* **105**, 115104 (2022).
42. Zhang, X.-J., Koch, E. & Pavarini, E. $LaVO_3$: a true Kugel-Khomskii system. *Phys. Rev. B* **106**, 115110 (2022).
43. Zhang, X.-J., Koch, E. & Pavarini, E. Origin of the transitions inversion in rare-earth vanadates. *Phys. Rev. Lett.* **135**, 026508 (2025).
44. Cwik, M. et al. Crystal and magnetic structure of $LaTiO_3$: evidence for nondegenerate t_{2g} orbitals. *Phys. Rev. B* **68**, R060401 (2003).
45. Ulrich, C. et al. Magnetic order and dynamics in an orbitally degenerate ferromagnetic insulator. *Phys. Rev. Lett.* **89**, 167202 (2002).
46. Sage, M. H., Blake, G. R., Nieuwenhuys, G. J. & Palstra, T. T. M. Evidence for electronic phase separation between orbital orderings in $SmVO_3$. *Phys. Rev. Lett.* **96**, 036401 (2006).
47. Blake, G. R., Palstra, T. T. M., Ren, Y., Nugroho, A. A. & Menovsky, A. A. Transition between orbital orderings in YVO_3. *Phys. Rev. Lett.* **87**, 245501 (2001).
48. Reehuis, M. et al. Structural and magnetic phase transitions of the orthovanadates RVO$_3$ (R=Dy, Ho, Er) as seen via neutron diffraction. *Phys. Rev. B* **83**, 064404 (2011).
49. Saha, R., Fauth, F., Caignaert, V. & Sundaresan, A. Coexistence of G- and C-type orbital ordered phases and its correlation with magnetization reversal in YVO_3. *Phys. Rev. B* **95**, 184107 (2017).
50. Reehuis, M. et al. Crystal and magnetic structure of $CeVO_3$ and $TbVO_3$. *Eur. Phys. J. B* **64**, 27 (2008).
51. Miyasaka, S., Okimoto, Y., Iwama, M. & Tokura, Y. Spin-orbital phase diagram of perovskite-type RVO$_3$ (R= rare-earth ion or Y). *Phys. Rev. B* **68**, 100406(R) (2003).
52. Zhou, J.-S., Goodenough, J. B., Yan, J.-Q. & Ren, Y. Superexchange Interaction in orbitally fluctuating RVO$_3$. *Phys. Rev. Lett.* **99**, 156401 (2007).
53. Muñoz, A. et al. Crystallographic and magnetic transitions in $CeVO_3$: a neutron diffraction study. *Phys. Rev. B* **68**, 144429 (2003).
54. Reul, J., Nugroho, A. A., Palstra, T. T. M. & Grüninger, M. Probing orbital fluctuations in RVO$_3$ (R=Y, Gd, or Ce) by ellipsometry. *Phys. Rev. B* **86**, 125128 (2012).
55. De Raychaudhury, M., Pavarini, E. & Andersen, O. K. Orbital fluctuations in the different phases of $LaVO_3$ and YVO_3. *Phys. Rev. Lett.* **99**, 126402 (2007).
56. Autieri, C., Koch, E. & Pavarini, E. Mechanism of structural phase transitions in $KCrF_3$. *Phys. Rev. B* **89**, 155109 (2014).
57. Yavas, H. et al. Direct imaging of orbitals in quantum materials. *Nat. Phys.* **15**, 559 (2019).
58. Leedahl, B. et al. Origin of Ising magnetism in $Ca_3Co_2O_6$ unveiled by orbital imaging. *Nat. Commun.* **10**, 5447 (2019).
59. Blaha, P., Schwarz, K., Sorantin, P. & Trickey, S. Full-potential, linearized augmented plane wave programs for crystalline systems. *Comp. Phys. Comm*. **59**, 399 (1990).
60. Musshoff, J., Kiani, A. & Pavarini, E. Magnetic response trends in cuprates and the $t-t'$ Hubbard model. *Phys. Rev. B* **103**, 075136 (2021).
61. Jülich Supercomputing Centre. JURECA: data centric and booster modules implementing the modular supercomputing architecture at jülich supercomputing centre. *J. Large Scale Res. Facilities* **7**, A182. https://doi.org/10.17815/jlsrf-7-182 (2021).

Acknowledgements

We would like to acknowledge computational time on the supercomputer JURECA[61], Forschungszentrum Jülich, and on the GCS supercomputer JUWELS (www.gauss-centre.eu) through NIC at the Jülich Supercomputing Centre.

Author contributions

E. K. and E. P. designed the study, wrote and approved the manuscript.

Funding

Open Access funding enabled and organized by Projekt DEAL.

Competing interests

The authors declare no competing interests.

Additional information

Correspondence and requests for materials should be addressed to Eva Pavarini.

Reprints and permissions information is available at http://www.nature.com/reprints

Publisher's note Springer Nature remains neutral with regard to jurisdictional claims in published maps and institutional affiliations.

Open Access This article is licensed under a Creative Commons Attribution 4.0 International License, which permits use, sharing, adaptation, distribution and reproduction in any medium or format, as long as you give appropriate credit to the original author(s) and the source, provide a link to the Creative Commons licence, and indicate if changes were made. The images or other third party material in this article are included in the article's Creative Commons licence, unless indicated otherwise in a credit line to the material. If material is not included in the article's Creative Commons licence and your intended use is not permitted by statutory regulation or exceeds the permitted use, you will need to obtain permission directly from the copyright holder. To view a copy of this licence, visit http://creativecommons.org/licenses/by/4.0/.

© The Author(s) 2026